Soil & Tillage Research 200 (2020) 104611

Contents lists available at ScienceDirect

Soil & Tillage Research

journal homepage: www.elsevier.com/locate/still

Soil compaction impacts soybean root growth in an Oxisol from subtropical Brazil

Moacir Tuzzin de Moraes[a,*], Henrique Debiasi[b], Julio Cezar Franchini[b], Alexandra Antunes Mastroberti[c], Renato Levien[d], Daniel Leitner[e], Andrea Schnepf[f]

[a] Federal University of Technology-Paraná, Campus Francisco Beltrão, Department of Agronomic Science, PO Box 135, 85601-970, Francisco Beltrão, PR, Brazil
[b] Embrapa Soybean, PO Box 231, 86001-970, Londrina, PR, Brazil
[c] Federal University of Rio Grande do Sul, Institute of Biosciences, Botany Department, Laboratory of Plant Anatomy, Campus do vale, 91509-900, Porto Alegre, RS, Brazil
[d] Federal University of Rio Grande do Sul, Faculty of Agronomy, Department of Soils, 91540-000, Porto Alegre, RS, Brazil
[e] Simulationswerkstatt, Ortmayrstrasse 20, 4060 Leonding, Austria
[f] Forschungszentrum Juelich GmbH, Institute of Bio- and Geosciences, IBG-3: Agrosphere, 52428 Juelich, Germany

ARTICLE INFO

Keywords:
Root growth modelling
Mechanical stress
Hydric stress

ABSTRACT

Soil mechanical impedance, hypoxia and water stress are the main soil physical causes of reduced root growth, but they are rarely included in root growth models. The aim of this work was to study the impact of soil compaction on soybean root growth in an Oxisol using extensive field data as well as a mechanistic model that is sensitive to soil physical conditions. Soybean was cultivated under field conditions in a Rhodic Eutrodox in four treatments. The treatments consisted of three soil compaction levels (no-tillage system, areas trafficked by a tractor, and trafficked by a harvester) and soil chiselling management (performed in an area previously cultivated under no-tillage). Soil structural properties (soil penetration resistance, bulk density, total porosity, macroporosity and microporosity), root system parameters (root length density, root dry mass and root anatomy) and crop production components (grain yield, shoot dry biomass) were determined for the four treatments down to 50 cm soil depth. A mechanistic model, sensitive to mechanical and hydric stresses, was applied to simulate soybean root growth. The model was able to simulate the interaction between the soil physical conditions and soybean root growth. Soil compaction differentiated vertical root distribution according to a stress reduction function impeding root elongation. Consequently, root growth was influenced by soil physical conditions during the cropping season, and simulated root length density showed strong agreement to measured data. Soybean grain yield was reduced due to both compaction (caused by harvester traffic) and excessive loosening (promoted by chiselling) relative to the no-tillage system. Soil physical attributes (i.e., soil bulk density, penetration resistance, macroporosity and microporosity) were only weakly correlated with grain yield and root growth. This may be due to the fact that those soil physical attributes are static properties that do not represent the dynamics of mechanical and hydric stresses during the growing season. Soil compaction changed the anatomy, shape and size of roots. Moreover, cortex cells were deformed in the secondary root growth stage. In the compacted soil, mechanical impedance had a major effect on root growth, while in the loose soil, the matric potential (water stress) represented the major soil physical limitation to root growth. Soil chiselling increased the root length density, but it reduced the grain yields due water stress. The study showed that soybean root growth was successfully modelled with respect to soil physical conditions (mechanical impedance, hypoxia and water stress) for different compaction levels of a Rhodic Eutrudox.

1. Introduction

Soil compaction is a frequent problem in arable soils, and even persists in no-tillage systems. In general, the compacted soil layer is located from 7 to 20 cm depth, and is caused by absence of crop rotation and crop residues or occurs due to inadequate soil chiselling (Nunes et al., 2015). Therefore, fixed shank openers working down to 17 cm depth, promoted physical improvement to the soil, favouring the

* Corresponding author.
E-mail addresses: mtmoraes@utfpr.edu.br (M.T.d. Moraes), henrique.debiasi@embrapa.br (H. Debiasi), julio.franchini@embrapa.br (J.C. Franchini), alexandra.mastroberti@ufrgs.br (A.A. Mastroberti), renatole@ufrgs.br (R. Levien), daniel.leitner@simwerk.at (D. Leitner), a.schnepf@fz-juelich.de (A. Schnepf).

https://doi.org/10.1016/j.still.2020.104611
Received 27 March 2019; Received in revised form 17 February 2020; Accepted 18 February 2020
Available online 02 March 2020

development of corn plants, and presenting potential to mitigate the compaction of clayey soils under no-tillage (Nunes et al., 2015). In this compacted soil layer the soil penetration resistance is increased (Moraes et al., 2016) limiting rooting depth and the soil volume used by roots for water (Nosalewicz and Lipiec, 2014) and nutrient uptake (Schnepf et al., 2012). Thus, a highly compacted soil layer (i.e. pan soil layers at 10 − 20 cm depth) increases the soil strength and results in a higher concentration of roots in the layer above and in reduced rooting in deeper layers due to the limitation for root growth or the absence of continuous macropores throughout the soil profile (Bengough, 2012; Nosalewicz and Lipiec, 2014). Soil compaction affects pore size distribution (Moraes et al., 2016), pore geometry, hence, gas and water fluxes and also root elongation (Bengough et al., 2011), and root system development (Chen and Weil, 2011).

The most commonly used soil physical indicators are bulk density, macroporosity and soil penetration resistance (Keller et al., 2015). However, the restrictive values of soil physical indicators should be adjusted both with respect to soil texture and tillage system (Reichert et al., 2009). Nevertheless, the critical thresholds of these soil physical indicators are not well known due to the fact that in many cases their correlations to plant development and grain yield are weak (Moraes et al., 2014a; Rabot et al., 2018) because the soil-plant-atmosphere system is dynamic. It shows daily variations of factors that affect the crop production directly (soil water content, soil penetration resistance, aeration, and temperature). Thus, for plant development the occurrence of stress conditions over time is more important than considering a fixed number of static soil physical properties.

Soil biophysical modelling of the soil-plant-atmosphere system can be used to determine the total stress that crops are exposed to during the growing season (Bengough, 1997). The sum of stresses during the season could reveal the real conditions for root and shoot development. For the understanding of the dynamics of soil physical processes that limit root growth, it is necessary to consider all stresses that affect plant growth (Bengough et al., 2011). Recently, a new model for coupling soil physical limitations to root growth was introduced to simulate the daily effects of mechanical and hydric stresses to root elongation during the growing season (Moraes et al., 2018). The approach uses the root architecture model RootBox (Leitner et al., 2010) to simulate root architecture in 3-D coupled with a model of the soil-root-plant-atmosphere system (Tron et al., 2015) to predict the root growth as a result of soil physical conditions (Moraes et al., 2018). To validate the new model it should be applied for different soil compaction levels.

We hypothesised that soybean root growth can be modelled as a function of soil physical limitations (mechanical impedance, hypoxia, and water stress) under various compaction levels of an Oxisol. The aim of this work was to study the impact of soil compaction on soybean root growth in an Oxisol from Subtropical conditions in Brazil based on the combined use of field data and modelling.

2. Material and methods

2.1. Study site

This experiment was setup in an area with a no-tillage system established in 1991 at the Experimental Station of Embrapa Soybean, in Londrina (latitude 23°12′S; longitude 51°11′W; and 585 m altitude State of Paraná, Southern Brazil. According to the Köppen classification, the climate of the region is humid subtropical Cfa, with annual average temperature of 21 °C and 1650 mm rainfall Alvares et al., 2013). The experiment was established on an Oxisol (Latossolo Vermelho Distroférrico, Brazilian classification; Rhodic Eutrudox, USA classification) with 784 g kg^{-1} of clay, 145 g kg^{-1} of silt and 71 g kg^{-1} of sand at 0 − 30 cm depth. Soil particle density at the same depth is 2.96 Mg m^{-3}, and the mean slope of the experimental area is 0.03 m m^{-1}. Before the establishment of the experiment, the area had been cropped, from 1991 to 2009, with a crop rotation system using soybean or maize in the summer and wheat or black oat in the winter. In the years 2010–2012, this area was cropped with *Urucloa ruziziensis* (as cover crop) without pasture, which was desiccated with herbicide at 90 and 20 days before establishment of treatments.

2.2. Experimental design and treatments

The field experiment was established in February 2013; the treatments were distributed in a randomized block design with four treatments and twelve replications. The treatments consisted of three compaction levels and soil chiselling management (performed in an area previously cultivated under no-tillage) in 5 m wide and 15 m long plots: minimum tillage with chiselling (MTC), no-tillage system (NT), and no-tillage with additional compaction by four passes of tractor (NTC4) or eight passes of harvester (NTC8).

Soil chiselling was performed in February of 2013, with the soil at friable consistency (gravimetric water content of 0.29 kg kg^{-1} in the 0–20 layer), by chisel plow equipped with five shanks spaced 35 cm relative to each other, and a shovel of 8 cm width, working at 25 cm depth.

The additional compaction on treatment NTC4 was performed in February 2013, with a tractor CBT 4 × 2 TDA, model 8060, equipped with an additional shovel/shell. The front tires were of type Goodyear 14.9–24 R1, while the rear tires were of type Goodyear 18.4–34 R1 ballasted with iron and liquid. The total mass of the tractor was 7.2 Mg.

Soil compaction in NTC8 was performed with a self-propelled grain harvester SLC-6200 (weight of 66 kN) equipped with a grain header for maize (weight of 12 kN), and with the grain tank empty, presenting a total weight of 78 kN (58 kN on the front axle). The total mass of the harvester was 9.5 Mg. The harvester was equipped with single front tires, Pirelli 18.4–30 R1, diagonals, inflated to a pressure of 180 kPa, and rear tires Pirelli 9.00–16 F2 10PR, diagonals, inflated to a pressure of 410 kPa. The ground pressure of the front tires was estimated to be 200 kPa, using a simple procedure proposed by O'Sullivan et al. (1999). Following this methodology, the soil-tire contact area was estimated from tire width and diameter, inflation pressure and load, using an empirical model developed for a rigid surface. The soil gravimetric water content during the tractor and harvester traffic was equivalent to field capacity (0.34 kg kg^{-1}).

2.3. Crop and field management

Soybean (cultivar BRS 359RR) was sown on 10th October 2013, with a seed drill (Jumil, Exacta 5070 model), equipped with shanks and double-disks as furrow openers for fertilizer (fertilizer metering mechanism with feed screw) and seed deposition (precision vacuum seeder with vertical plates). The crop was seeded at a density of 30 plants m^{-2} (i.e. 13.5 plants m^{-1} row) with an inter-row spacing of 45 cm, and at a depth of 5 cm. The fertilizer (NPK 0-20-20, 270 kg ha^{-1}) was applied in-furrow 5 cm below and 5 cm to the side of the seed using the shanks working at 10 cm depth. The sowing, crop management, control of weeds, pests, and diseases followed the technical recommendations for the cultivation of soybean (Embrapa, 2011) and were the same for all treatments.

2.4. Soil sampling

The soil was sampled in all treatments in April 2013, after the soil compaction or soil chiselling. Undisturbed soil cores (internal diameter of 5.0 cm, and a height of 5.0 cm) were collected in five soil layers at intervals of 10 cm depth in duplicates, totalling 480 samples. The cores were sampled at soil water content near field capacity, by means of a soil sampler apparatus coupled to a tractor, enabling the vertical insertion of the core in the centre of each soil layer.

2.5. Determination of soil physical and hydraulic properties

Soil water retention curve and soil penetration resistance curve were determined by separating of soil cores into six groups with 80 samples, 480 soil samples in total. Samples were gradually saturated with distilled water, separated into groups, and then placed on tension tables and Richards' pressure chambers until the drainage ceased. Each sample group was subject to a matric potential (i.e., −3 and −6 kPa on a tension table, and −10, −33, −100, and −500 kPa using Richards' pressure chambers). After reaching equilibrium at each matric potential, the soil penetration resistance was measured with a lab penetrometer (Moraes et al., 2014b). Soil samples were weighed and all samples were oven-dried at 105 °C for 48 h to quantify the soil dry bulk density (Mg m^{-3}) and volumetric soil water content (m^3 m^{-3}). The soil total porosity (m^3 m^{-3}) was obtained by the relationship between bulk density and soil particle density (2.96 Mg m^{-3}), while the macroporosity (pores > 50 mm) was calculated as the difference between total porosity and soil microporosity (pores < 50 mm, equivalent to the soil water content at matric potential of −6 kPa, equilibrated in tension table).

2.6. Soil penetration resistance in the field

Soil penetration resistance was measured in the field at the end of the soybean season on 26 February 2014. For this purpose, we measured the soil penetration resistance at ten points at a spacing of 9 cm (two transects of 45 cm length) on a transect transversal to the soybean row, totalling in 120 measurement points. The digital penetrometer was equipped with a tip cone composed of a base area of 130 mm^2 and a solid angle of 30°, and the vertical measurement interval was 1 cm. Soil water content was determined along each plot by a disturbed soil sampler in five soil layers, each 10 cm until 50 cm depth.

2.7. Grain yield and shoot dry weight

The soybean grain yields were evaluated by mechanical harvest from 12 m of six central rows within each plot, with a total area of 32.4 m^2. The seeds were cleaned and weighed; and the values obtained were adjusted to 13 % moisture content. The shoot dry weight was measured twice at the 49th (28 November 2013) and 89th (07 January 2014) day after sowing. For this purpose, plants in two rows with 100 cm length were sampled and dried in an oven at 60 °C.

2.8. Root system sampler and analyses

Root system sampling was performed on the 5th January of 2014 at 87 days after soybean sowing. Soil monoliths were sampled for soybean root distribution throughout the soil profile (until 50 cm depth) in four of the twelve replications for each of the four treatments, totalling 16 trenches. Root analysis was performed for each soil sample by a simple spade method that requires taking a soil monolith and separating the soil from the roots by washing (Böhm, 1979). These monoliths (7 cm thick) were sampled in trenches perpendicular to the soybean seedling row (45 cm) until 50 cm depth. Each monolith (50 × 45 × 7 cm) was subdivided into five depths (0–10, 10–20, 20–30, 30–40, and 40 − 50 cm) at five positions perpendicular to the crop row (each 9 cm, i.e. 0–9, 9–18, 18–27, 27–36, 36 − 45 cm), resulting in 25 soil blocks for each field replicate, totalling in 400 samples.

The total root length was estimated by scanning approximately 10 % of root mass from each soil block as suggested in Costa et al. (2000). The images were prepared by spreading the roots on a transparent glass tray (20 × 30 cm) with a 3-mm water layer. Root length was obtained by scanning the root samples in a scanner (Delta-T Scan) followed by image processing using a software for analysis of fragments and roots, Safira 2.0 (Jorge and Silva, 2010). Based on the root length, root length density was calculated as the ratio of root length/soil volume (cm cm^{-3}). To determine root dry weight, the washed and cleaned roots were dried in an oven at 60 °C for 96 h. Root weight density (g m^{-2} in 10 cm depth) was calculated by relating root dry mass and sampled soil surface area.

2.9. Root anatomy analysis

Histological analyses were performed on soybean roots at the same time of the root length density analyses (87 days after sowing).The soybean root fragments (lateral roots) with approximately 5 cm length were sampled in the field at 4.5–13.5 cm distance from the plant stem and located within the top 10 cm depth. The roots were fixed in a solution of 4% paraformaldehyde and 4% glutaraldehyde in sodium phosphate buffer (0.1M pH 7.2) for 24 h and then water was removed stepwise by passing the root specimens through ethanol solutions with increasing concentrations (every 10 %) from 10 % to 100 % (15 min each) at room temperature. Afterwards the roots were embedded in Hydroxiethylmethacrylate resin (historesin kit). The microscope slides were made on cross sections of the longitudinal root axis with 1 μm thickness. Ten cross sections of root were performed using a rotary microtome Leica with approximately 1 μm thickness, and subsequently stained with toluidine blue O (C.I. 52040), pH 4.4 (O'Brien et al., 1964). Permanent slides were analysed by a light microscope in bright field (Olympus BX41).

2.10. Climatic data

Climatic data during the soybean season (from October 2013 to March 2014) were collected from the weather station at the Embrapa Soybean, near the experiment at field. Thus, weather data were collected daily, in measurement interval of 15 min, for solar radiation, temperature, relative humidity, wind speed and precipitation during the development of the crop. The reference evapotranspiration was calculated from the meteorological data using the Penman-Monteith equation (Allen et al., 1998).

2.11. Root growth modelling

Root growth was modelled in the MATLAB® programming language. The effects of the soil physical limitations on root elongation (stress reduction function) proposed by Moraes (2017) was incorporated into the RootBox model of root architecture (Moraes et al., 2018). Thus, the 3-D root growth model was coupled to a 1-D soil water flow model that solves the Richards equation following van Dam and Feddes, 2000 and the root water absorption model proposed by De Jong Van Lier et al. (2008).

The root elongation is impeded by a combination of water stress, poor aeration, and soil strength, and is predicted by a stress reduction function (Moraes et al., 2018). The root elongation rate is reduced due to the influence of soil strength with an exponential relationship (Bengough, 1997) considering the presence of continuous macropores at the soil profile (Moraes et al., 2018). Thus, root elongation is represented as a function of soil strength and matric potential, which may vary in time and depth. The model equations as well as the coupling and numerical implementation are described in Moraes et al. (2018).

2.12. Soil strength as a function of water content and bulk density

Soil penetration resistance varies greatly with soil water status, and was modelled as a function of soil water content and bulk density using a non-linear model (Eq. (1)) (Busscher, 1990). The constants *a, b,* and *c* are found by fitting Eq. (1) to the experimental values of soil penetration resistance, water content and bulk density (Moraes et al., 2017).

$$Q_p = a\,\gamma^b \theta^c \quad (1)$$

where Q_p (MPa) is the soil penetration resistance; γ (g cm^{-3}) is the dry bulk density; θ (cm^3 cm^{-3}) is volumetric soil water content and *a, b* and *c* are empirical parameters. For this soil (Rhodic Eutrudox) we used the parameters a = 0.00587; b = 8.0772; and c = −4.65 (Moraes et al., 2019).

2.13. Root elongation as a function of soil physical stresses

Root elongation was described as a function of both soil strength and matric potential. We further assumed that the combined effect of the two stresses (mechanical and hydric stress) is multiplicative for each time and depth, i.e., the decrease elongation rate can be described by Eqs. (2) and (3) (Moraes et al., 2018). Thus, root elongation can be represented as a function of soil strength (Q_p) and matric potential (h), at time (t) and depth (z) (Eq. (3)).

$$RE(Q_p, h)_{t,z} = srf(Q_p, h)_{t,z}\, RE_{max} \quad (2)$$

$$srf(Q_p, h)_{t,z} = \alpha(Q_p)_{t,z}\, \alpha(h)_{t,z} \quad (3)$$

where $srf(Q_p, h)_{t,z}$ is the total stress reduction function for root elongation due to mechanical (Q_p) and water (h) stresses in each time (t) and depth (z); $\alpha(Q_p)$ is the stress reduction function based on soil strength and is given by Eq. (4) for a soil with continuous macropores (Moraes et al., 2018); α(h) is the stress reduction function based on matric potential (water and aeration stress) given by Eq. (5) and, t is the time (day), z is the depth (cm); RE_{max} is the unimpeded root elongation (cm day^{-1}), and RE is the root elongation (cm day^{-1}).

2.14. Root elongation in relation to soil strength

We used soil penetrometer resistance, which depends on water content and bulk density, as a measure of soil strength. Root elongation reduction due to strength-induced stress in layer z, on day t, is given by Eq. (4) following the recommendation for a soil with continuous pores in the soil profile (Moraes et al., 2018).

$$\alpha(Q_p)_{t,z} = exp(-0.30\, Q_p), \quad (4)$$

where Q_p is soil penetration resistance (MPa); $\alpha(Q_p)$ is the stress reduction function by soil strength; t is the time (day), and z is the depth (cm).

2.15. Root elongation under water stress and poor aeration

Under non-optimal hydric conditions, i.e., either too dry (water stress) or too wet (poor aeration), the root elongation is reduced by means of the stress reduction factor α(h), ranging from 1 (maximum root elongation) to zero (no growth) (Moraes et al., 2018). The relationship between root elongation rate and matric potential is described by Eq. (5) in terms of five stages: (1) no root growth due to anoxic conditions $|h| < |h_1|$; (2) root elongation rate increases linearly from $|h_1|$ an $|h_2|$, due to improved soil aeration; (3) no hydric stress of root elongation from $|h_2|$ to $|h_3|$ (4) root elongation rate was reduced linearly due to water stress from $|h_3|$ to $|h_4|$; (5) no root growth due to water stress when $h > |h_4|$. The h_1 value (-0.1 kPa) was defined at the wet end and represents the start of water drainage and increase of soil aeration (and oxygen concentration) necessary for root growth (Dresbøll et al., 2013; Saglio et al., 1984). The h_2 (−6 kPa) and h_3 (−10 kPa) were the values close to optimal matric potential for root growth (Iijima and Kato, 2007), when there is neither water stress or poor aeration. The h_4 (−1000 kPa) was defined as the limit of maximum growth due to turgor pressure in the expanding cells of the root elongation zone (Bengough et al., 2011).

Table 1
Van Genuchten's parameter, hydraulic conductivity, bulk density and degree of compaction of a Rhodic Eutrudox for four compaction levels: minimum tillage with chiselling (MTC) no-tillage (NT) no-tillage with four tractor passes (NTC4) no-tillage with eight harvester passes (NTC8).

Depth cm	θ_s cm^3 cm^{-3}	θ_r cm^3 cm^{-3}	α cm^{-1}	n –	K_s cm day^{-1}	γ g cm^{-3}	DC %
	MTC						
0–10	0.585	0.198	0.1927	1.2691	83.78	1.10	72
11–20	0.553	0.200	0.1313	1.1839	83.78	1.16	76
21–30	0.526	0.200	0.0469	1.1469	57.26	1.27	83
31–40	0.550	0.200	0.0512	1.1654	35.70	1.16	76
41–50	0.554	0.198	0.0583	1.1679	44.70	1.10	72
51–80*	0.558	0.200	0.1119	1.1640	44.70	1.08	71
81–100*	0.566	0.214	0.0930	1.2105	44.70	1.05	69
	NT						
0–10	0.555	0.198	0.0892	1.1848	39.36	1.21	79
11–20	0.537	0.200	0.0822	1.1503	39.36	1.26	82
21–30	0.539	0.200	0.0756	1.1407	54.15	1.26	82
31–40	0.539	0.200	0.0756	1.1407	54.15	1.16	76
41–50	0.539	0.200	0.0756	1.1407	54.15	1.08	71
51–80*	0.558	0.200	0.1119	1.1640	44.70	1.08	71
81–100*	0.566	0.214	0.0930	1.2105	44.70	1.05	69
	NTC4						
0–10	0.508	0.200	0.0128	1.1782	26.09	1.35	88
11–20	0.510	0.200	0.0252	1.1391	26.09	1.34	87
21–30	0.524	0.197	0.0180	1.1494	26.98	1.32	86
31–40	0.550	0.200	0.0512	1.1654	35.70	1.16	76
41–50	0.554	0.198	0.0583	1.1679	44.70	1.10	72
51–80*	0.558	0.200	0.1119	1.1640	44.70	1.08	71
81–100*	0.566	0.214	0.0930	1.2105	44.70	1.05	69
	NTC8						
0–10	0.499	0.200	0.0017	1.2480	18.39	1.39	91
11–20	0.505	0.200	0.0102	1.1485	18.39	1.37	90
21–30	0.526	0.200	0.0211	1.1307	15.29	1.33	87
31–40	0.550	0.200	0.0512	1.1654	35.70	1.16	76
41–50	0.554	0.198	0.0583	1.1679	44.70	1.10	72
51–80*	0.558	0.200	0.1119	1.1640	44.70	1.08	71
81–100*	0.566	0.214	0.0930	1.2105	44.70	1.05	69

θr, θs, α, and n are van Genuchten's parameters; Ks: saturated hydraulic conductivity; γ: soil bulk density; DC: degree of compaction.

* Soil physical attributes, hydraulic properties and van Genuchten parameters at soil layers from 50 to 100 cm depth were sampled in no-tillage system described in Ortigara (2017).

$$\alpha(h)_{t,z} = \begin{cases} 0 & if \quad |h| \le |h_1| \\ \dfrac{(|h_1| - |h|)}{(|h_1| - |h_2|)} & if \quad |h_1| < |h| \le |h_2| \\ 1 & if \quad |h_2| < |h| \le |h_3| \\ \dfrac{(|h_4| - |h|)}{(|h_4| - |h_3|)} & if \quad |h_3| < |h| \le |h_4| \\ 1 & if \quad |h| > |h_4| \end{cases} \quad (5)$$

where α(h) is the stress reduction factor of root elongation due to pressure head; |h| is the module of pressure head, and h_1, h_2, h_3 and h_4 are the limits of pressures head for root elongation (described above).

2.16. Input and output data

The input parameters of the model were the soil characteristics (soil water retention curve, soil penetration resistance curve, saturated hydraulic conductivity and soil bulk density) (Table 1), climate characteristics (evaporation and potential transpiration, air temperature, air humidity, precipitation and irrigation) and crop root characteristics (length of apical and basal zone, spacing between branches, number of branches and root insertion angle), type of tropism, period of growth, physical limitations of resistance, and matric potential for root elongation (Table 2). The input parameters for the soybean root system architecture follow the values calibrated for this crop and soil in Moraes et al. (2018). In addition, we used the soil physical attributes, hydraulic

Table 2
Root architectural parameters of soybean (*Glycine max*).

Symbol	Parameter name	units	Values[1] [mean, s.d.]
Tap root			
r_e	Initial tip elongation rate	cm day^{-1}	[5.5, 0]
a	Root radius	cm	[0.2, 0]
l_a	Length of apical zone	cm	[2.0, 0]
l_b	Length basal zone	cm	[1.0, 0]
l_n	Internodal distance	cm	[0.65, 0]
n_b	Maximum number of branches	–	[300, 0]
σ	Expected change of root tip heading	rad cm^{-1}	0.4
type	Type of tropism	–	1
N	Strength of tropism	–	1.5
dx	Spatial resolution along root axis	cm	0.25
First-order laterals			
r_e	Initial tip elongation rate	cm day^{-1}	[2, 0]
a	Root radius	cm	[0.04, 0]
Θ	Insertion angle	rad	[1.2217, 0]
l_a	Length of apical zone	cm	[3, 0]
l_b	Length basal zone	cm	[3, 0]
l_n	Internodal distance	cm	[0.7, 0]
n_b	Maximum number of branches	–	[50, 0]
σ	Expected change of root tip heading	rad cm^{-1}	0.3
type	Type of tropism	–	1
N	Strength of tropism	–	0.1
dx	Spatial resolution along root axis	cm	0.25
Second-order laterals			
r_e	Initial tip elongation rate	cm day^{-1}	[2, 0]
a	Root radius	cm	[0.02, 0]
Θ	Insertion angle	rad	[1.22173, 0]
k	Maximal root length	cm	[5, 0]
σ	Expected change of root tip heading	rad cm^{-1}	0.5
type	Type of tropism	–	1
N	Strength of tropism	–	0
dx	Spatial resolution along root axis	cm	0.25
Basal roots			
r_e	Initial tip elongation rate	cm day^{-1}	[3.5, 0]
a	Root radius	cm	[0.06, 0]
Θ	Insertion angle	rad	[1.5708, 0]
l_a	Length of apical zone	cm	[5, 0]
l_b	Length basal zone	cm	[2, 0]
l_n	Internodal distance	cm	[3, 0]
n_b	Maximum number of branches	–	[15, 0]
σ	Expected change of root tip heading	rad cm^{-1}	0.1
type	Type of tropism	–	1
N	Strength of tropism	–	0.5
dx	Spatial resolution along root axis	Cm	0.25

[1] Root parameter values are from Moraes et al. (2018) and calibrated for this experiment; s.d. is the standard deviation.

properties and van Genuchten (1980) parameters at soil layers from 50 to 100 cm depth sampled in the no-tillage system described in Ortigara (2017).

The results of the model are variables of the soil (water balance, infiltration, runoff and deep drainage, actual evaporation, water content, matric potential, soil mechanical resistance to penetration and unsaturated hydraulic conductivity) and the crop (root system distribution, root length density, actual transpiration and water uptake) over time for each soil layer. Root length density of soybean was calculated for each depth for a single plant in an area of 0.03 m^2 plant^{-1} (45 cm length and 7 cm width), i.e. with a plant density of 300,000 plants ha^{-1}.

In addition, as results of this root growth modelling, we obtained results of unsaturated hydraulic conductivity. The soil hydraulic functions θ(h) and K(θ) were estimated with Eqs. (6) and (7) as suggested by the Mualem-van Genuchten model (van Genuchten, 1980), described in van Dam and Feddes (2000), as part of this root growth model. Thus, as output of this root growth model we obtained the daily values of unsaturated hydraulic conductivity (K(θ)). Thus, for 0 − 10 cm depth, we related that K(θ) daily values with matric potential to derive the soil hydraulic function K(h) as suggested De Jong Van Lier et al. (2008).

$$\theta(h) = \theta_r + \left(\frac{\theta_s - \theta_r}{(1 + (|\alpha h|)^n)^{(1-1/n)}}\right) \quad (6)$$

$$K(\theta) = K_s\left(\frac{\theta - \theta_r}{\theta_s - \theta_r}\right)^{\lambda} \cdot \left(1 - \left(1 - \left(\frac{\theta - \theta_r}{\theta_s - \theta_r}\right)^{n/(n-1)}\right)^{(n-1)/n}\right)^2 \quad (7)$$

where, θ_s, θ_r, α and n are empirical parameters from the van Genuchten-Mualem model described at the Table 1. Ks is saturated hydraulic conductivity. The value of parameter λ was 0.5 (Mualem, 1976; van Genuchten, 1980).

2.17. Performance evaluation of the soybean root growth model

The agreement between the measured and simulated values was expressed by the mean absolute error (MAE) (Casaroli et al., 2010), the root-mean-square error (RMSE) (de Jong van Lier et al., 2008) and the coefficient of residual mass (CRM) (Bonfante et al., 2010). The precision was determined by the correlation coefficient (r) (Addiscott and Whitmore, 1987) and the accuracy by means of the Willmott concordance index (d) (Willmott et al., 2012), while the modelling performance was evaluated using the efficiency of the model (EF) (Bonfante et al., 2010) and the proximity of the 1:1 line.

2.18. Data analysis

The data of soil attributes (soil penetration resistance, bulk density, macroporosity, microporosity) and plant responses (grain yield, shoot production, root length density and root dry mass) were subjected to analysis of variance (ANOVA, F value, $p < 0.05$). ANOVA was performed separately for each layer. When the effects of the treatments were significant, means were compared with Tukey's test ($p < 0.05$). All data analysis was performed using the software, Statistical Analysis System 6.1 (SAS, 2013). Correlation of soil physical attributes (bulk density, macroporosity, microporosity and soil penetration resistance) with productivity or root length density was analysed with SigmaPlot® 12.0 (Systat software, Inc.).

3. Results

3.1. Soil physical properties

Soil penetration resistance was strongly affected by machinery traffic and soil chiselling (Fig. 1). Soil water content did not vary significantly between treatments and thus no effect of water dynamics on penetration resistance could be observed. In general, the water content ranged from 0.29 kg kg^{-1} (0 − 10 cm layer) to 0.37 kg kg^{-1} (40–50 layer). These values are near the field capacity for each soil layer. There were differences in the soil penetration resistance above 23 cm depth, and generally, the higher values appeared for NTC8 and the smaller ones for the soil chiselling. For all profiles, there were little differences between NT and NTC4. This could be due to the high observed water content. The soil bulk density (Fig. 2) of the top soil layer (0 − 10 cm) was different between treatments, in ascending order: MTC < NT < NTC4 < NTC8.

As expected, the machine traffic increased bulk density and

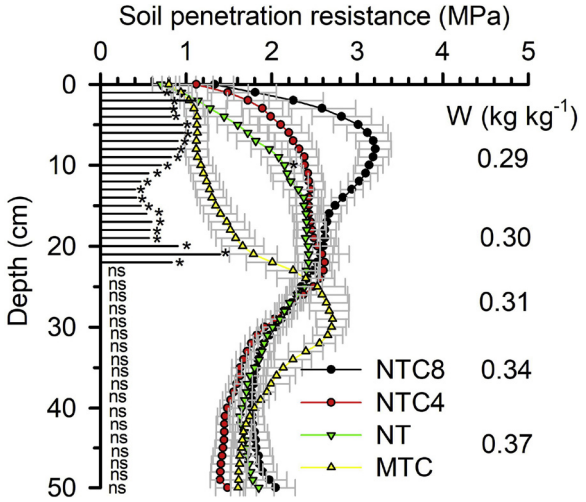

Fig. 1. Soil penetration resistance in a Rhodic Eutrudox under different compaction levels. MTC: minimum tillage system with soil chiselling; NT: no-tillage system; and no-tillage with additional compaction by four passes of tractor (NTC4) or eight traffic of harvester (NTC8). *: significant by minimum significant difference (bars) according to Tukey test ($p < 0.05$). ns: not significant. W: gravimetric water content.

microporosity in relation to no-tillage, and the soil chiselling decreased those values (Fig. 2). In addition, the microporosity and total porosity were reduced in compacted soil and increased in chiselled soil in relation to no-tillage. Four passes of the tractor or eight of the harvester increased the bulk density and decreased the total porosity for all layers above 30 cm depth. There was an effect of soil chiselling only down to 20 cm depth. As expected, soil chiselling increased the macroporosity and reduced the microporosity. Thus, there are differences in soil physical quality between compaction levels, especially at the 0–10 and 10 − 20 cm soil layers, potentially affecting root growth.

In addition, results showed that soil physical quality indicators with greater sensitivity to the different levels of soil compaction were macroporosity, soil penetration resistance and bulk density. It should be noted that soil penetration resistance tends to be more sensitive than determinations based on mass/volume ratios, to identify soil compaction effects in drier soil conditions (Moraes et al., 2013).

Soil unsaturated hydraulic conductivity related with matric potential revealed smaller values of unsaturated hydraulic conductivity in chiselled soil than in no-tillage or in areas with machinery traffic (Fig. 3a). Soil compaction due to machinery traffic in a previously structured soil increased the unsaturated hydraulic conductivity, compared with soil chiselled (Fig. 3b). Chiselled soil increased pore size compared to no-tillage (Fig. 2c and d), favouring the reduction of unsaturated hydraulic conductivity (Fig. 3b). During the growing season, the unsaturated hydraulic conductivity was greater in both in the no-tillage and in the compacted soil than in the loose soil, increasing unsaturated soil water flux for root water uptake.

3.2. Soybean grain yield

Grain yield of soybean was affected by compaction, and there was a strong negative response to compaction and chiselling (Fig. 4a). Results demonstrate that no-tillage was the best condition for soybean yield. Reduction on soybean grain yield due to soil compaction was observed in other studies, and is probably related to the reduced water availability caused by a smaller volume of soil that can be explored when root growth is restricted (Calonego and Rosolem, 2010).

Shoot dry weight, in two evaluations, was not affected by soil compaction levels (Fig. 4b). Plants produced around 1 Mg ha^{-1} of shoot dry weight at the 49th day (phenologic stadium R2), and more than 6 Mg ha^{-1} at the 89th day (phenologic stadium R5.5), probably as a result of adequate rainfall during that vegetative growing period (Fig. 5). Total rainfall was 372 mm during the crop growing season (126 days), with 44 days raining. However, there was 122 mm of rainfall in the vegetative stages (14 days of rain, until phenologic

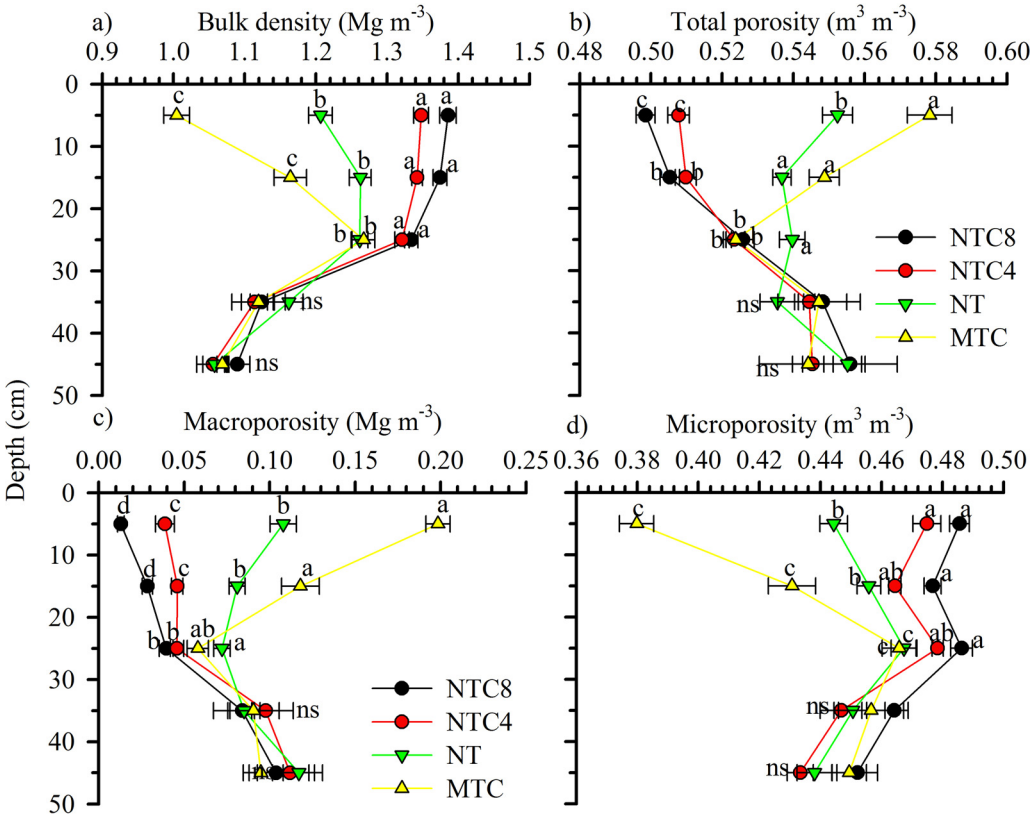

Fig. 2. Soil bulk density (a), total porosity (a), macroporosity (a), and microporosity (d) in profiles of a Rhodic Eutrudox under different compaction levels. MTC: minimum tillage system with soil chiselling; NT: no-tillage system; and no-tillage with additional compaction by four passes of tractor (NTC4) or eight passes of harvester (NTC8). *Means followed by same letter, in each soil layer, do not differ based on the Tukey test ($p < 0.05$). ns: not significant in each soil layer.

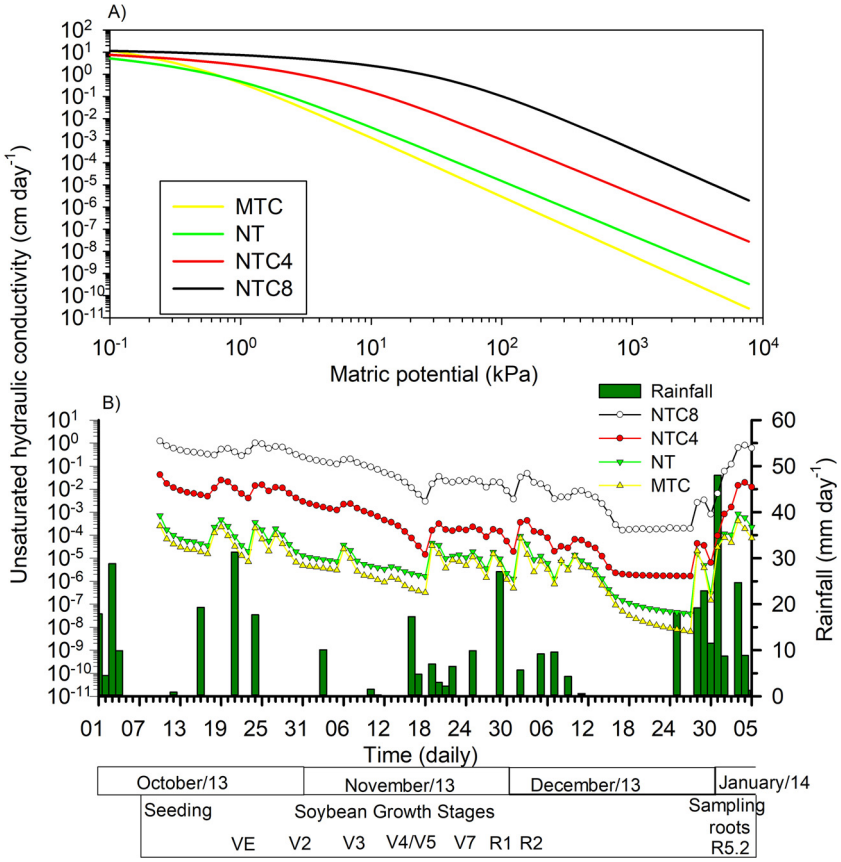

Fig. 3. Soil hydraulic conductivity as a function of matric potential at 0-10 cm depth (a) and soil unsaturated hydraulic conductivity simulated daily at 5 cm depth and rainfall during soybean season growth in four soil compaction levels of an Oxisol.

stadium V7), 230 mm at the reproductive stages from R1 to R5.2 (17 days of rain), and just 20 mm in 37 days (with only 13 days of rain) from seed stage (R5.2) to overmatured pod stage (R9).

3.3. Soybean root system

Root length density and root dry mass of soybean were affected by compaction levels (Fig. 6a–c), however there were no differences of root dry biomass at the 0 – 10 cm layer (Fig. 6a). For the top soil layer (0 – 10 cm) and second soil layer (10 – 20 cm) there was a higher total root length in the soil chiselling than in the other treatments. Furthermore, there was a lower root length density in NTC8 at the top layer than in all others treatments. For the root dry mass, there were differences at 10 – 20 cm and 30 – 40 cm. For the 10 – 20 cm, most root mass was found in the soil chiselling treatment, followed by NT. Already at 30 – 40 cm, there was a higher root mass in the NTC8 than in chiselled soil. In addition, positive soil chiselling effects were restricted down to 25 cm depth while root growth below 30 cm depth was restricted to soil compaction.

Thus, as expected, there was a higher root length density at lower soil compaction level, and the root distribution was different in the different treatments. For all treatments, the root distribution decreased exponentially with depth (Fig. 6b and c). There was reduction in root length density in the compacted layers. However, there was a higher root mass in deeper layers (30 – 40 cm) under harvest traffic (NTC8) than in the other treatments (Fig. 6a). This was probably due to root growth restriction in top soil layers, with increased root growth in deeper soil layers. Mean root length density measured in the field for all soil profiles (0 – 50 cm) was 2.42 cm cm^{-3} (chiselling) 1.94 cm cm^{-3} (no-tillage), 1.75 cm cm^{-3} (NTC4), and 1.79 cm cm^{-3} (NTC8). There

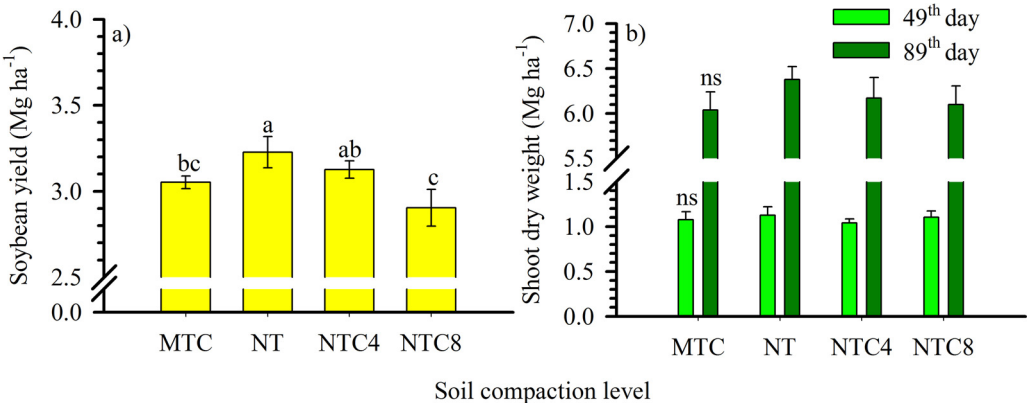

Fig. 4. Soybean grain yield (a) and shoot dry mass (b) as a function of soil compaction levels of Rhodic Eutrudox. MTC: minimum tillage system with soil chiselling; NT: no-tillage system; and no-tillage with additional compaction by four passes of tractor (NTC4) or eight passes of harvester (NTC8). *Means followed by the same letter do not differ according to the Tukey test ($p < 0.05$). ns: not significant. Vertical bars indicate standard error of the mean.

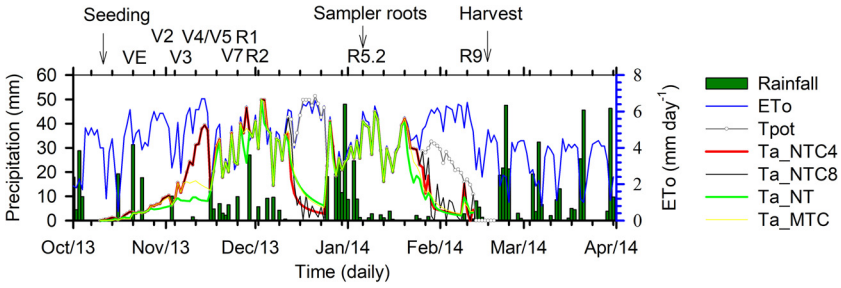

Fig. 5. Rainfall, reference evapotranspiration (ETo), potential transpiration (Tp), actual transpiration (Ta) for compaction levels, and phenological development stages of soybean. MTC: minimum tillage system with soil chiselling; NT: no-tillage system; and no-tillage with additional compaction by four passes of tractor (NTC4) or eight passes of harvester (NTC8).

were some indications that if the soil is compact at the surface, the mass of root was increased in the deeper loose soil layer, which was observed in the NTC8. For example, the root dry mass at the 30 – 40 cm depth, in NTC8 was 5.23 g m^{-2}/10 cm depth (1.38 cm cm^{-3}), against 3.32 g m^{-2}/10 cm depth (0.88 cm cm^{-3}) in soil chiselling. This indicates that there is a strong effect of soil physical conditions (i.e., mechanical and hydric stresses) impeding or favouring root growth in the soil profiles.

3.4. Relationship between soil physical properties and crop and root parameters

Soil physical attributes (soil bulk density, macroporosity, microporosity and penetration resistance at 0 – 20 cm depth) were significantly related with grain yield and root length density (Fig. 7). However, the R-square values in Fig. 7 show that physical properties alone do not explain the observed grain yield (Fig. 7a, c, e and g) and root growth variations (Fig. 7b, d, f and h). In general, the R-square values of the relationship of physical attributes and crop responses were smaller for grain yield (e.g., R-square of 0.23 between grain yield and soil penetration resistance) than for the root length density (e.g., R-squared of 0.61 between root length density and macroporosity). Grain yield could best be predicted by nonlinear regression using a quadratic equation for all attributes (bulk density, macroporosity, microporosity and soil penetration resistance).

In general, soybean grain yield was affected by soil chiselling or soil compaction. Relation of bulk density and productivity indicates that there are losses when the soil was loose or compact. For example, there was a reduction of 18 % of productivity when the soil is compacted (bulk density of 1.44 Mg m^{-3}), but, still there were 12 % of losses observed in a loose soil (bulk density 1.00 Mg m^{-3}). Maximum soybean grain yield was observed in the soil with a bulk density of 1.18 Mg m^{-3} (and a macroporosity of 11 %, a microposority of 41 % and a soil penetration resistance of 1.32 MPa). This bulk density value corresponds to the bulk density of the no-tillage system (Fig. 7a). In addition, there was higher variability in the data set, with small values of R-square for physical attributes and crop responses, due to the fact that the soil physical properties are static and not reflect the dynamics during the growing season.

Root length density was reduced exponentially with bulk density and microporosity (Fig. 7b and f). Root length density increased linearly with macroporosity, and decreased with increasing soil penetration resistance. However, the R-square of the regression between physical attributes and root length density were smaller than 0.61, indicating a weak relationship.

3.5. Root growth modelling

We simulated the root system development for the different soil compaction levels, and the resulting 3D root architectures at day 87 are presented in contour view (Fig. 8a-iii–d-iii). The 2D root distributions that were measured in the field (Fig. 8a-i–d-i) for all treatments agreed with the 2D root distribution obtained from the 3D model simulation results (Fig. 8a-ii–d-ii). Root length density decreases exponentially with depth (Fig. 6b and c), and there were horizontal variations in the root distribution (Fig. 8). Fig. 8c-iii and d-iii shows that root architecture was changed due to soil restrictions. In loose soil (soil chiselled), the root length density was higher, especially from zero to 20 cm depth (Fig. 8a). With increasing bulk density, and thus soil strength, root growth was strongly impeded (particularly in treatments NTC4 and NTC8) (Fig. 8c and d). As expected from the bulk density values shown in Fig. 2, there was an intermediate value of root length density in the no-tillage treatment (Fig. 8b). We included videos that visualize the dynamics of root growth and stress reduction function during the vegetation period for the minimum tillage system with soil chiselling (supplementary video S1), the no-tillage system (supplementary video S2), and for the no-tillage system with additional compaction by four passes of tractor (supplementary video S3) or eight passes of harvester (supplementary video S4).

From the simulated 3D root architecture, root length density values of the five soil layers were computed and compared with the ones measured in the field. For the four compaction levels (Fig. 9), the values of root mean square error (RMSE = 0.84), coefficient of correlation (r = 0.87), modelling efficiency (EF = 0.78), and coefficient of agreement of Willmott (d = 0.95), indicated strong agreement between simulated and measured root length densities. This implies that the dynamic soil physical conditions that had occurred during the cropping season and their effect on root growth had been well represented in the model. In the no-tillage treatment, there were fewer days with increased restriction for root elongation (Fig. 10) than in the compacted soil treatments.

Rooting depths are shown by the dashed lines in Fig. 10. In the soil chiselling treatment, the root system needed 37 days to reach 50 cm

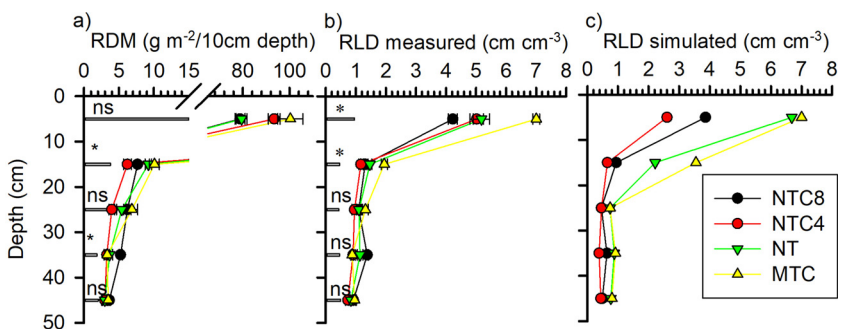

Fig. 6. Distribution of soybean root dry mass (a), and root length density measured in the field (b) and simulated (c) under different soil compaction levels in a Rhodic Eutrudox. *Bars are the minimum significant difference. ns: not significant in each soil layer. *There are differences between treatments based on Tukey test ($p < 0.10$). RDM: root dry mass; RLD: root length density; MTC: minimum tillage system with soil chiselling; NT: no-tillage system; and no-tillage with additional compaction by four passes of tractor (NTC4) or eight passes of harvester (NTC8), respectively.

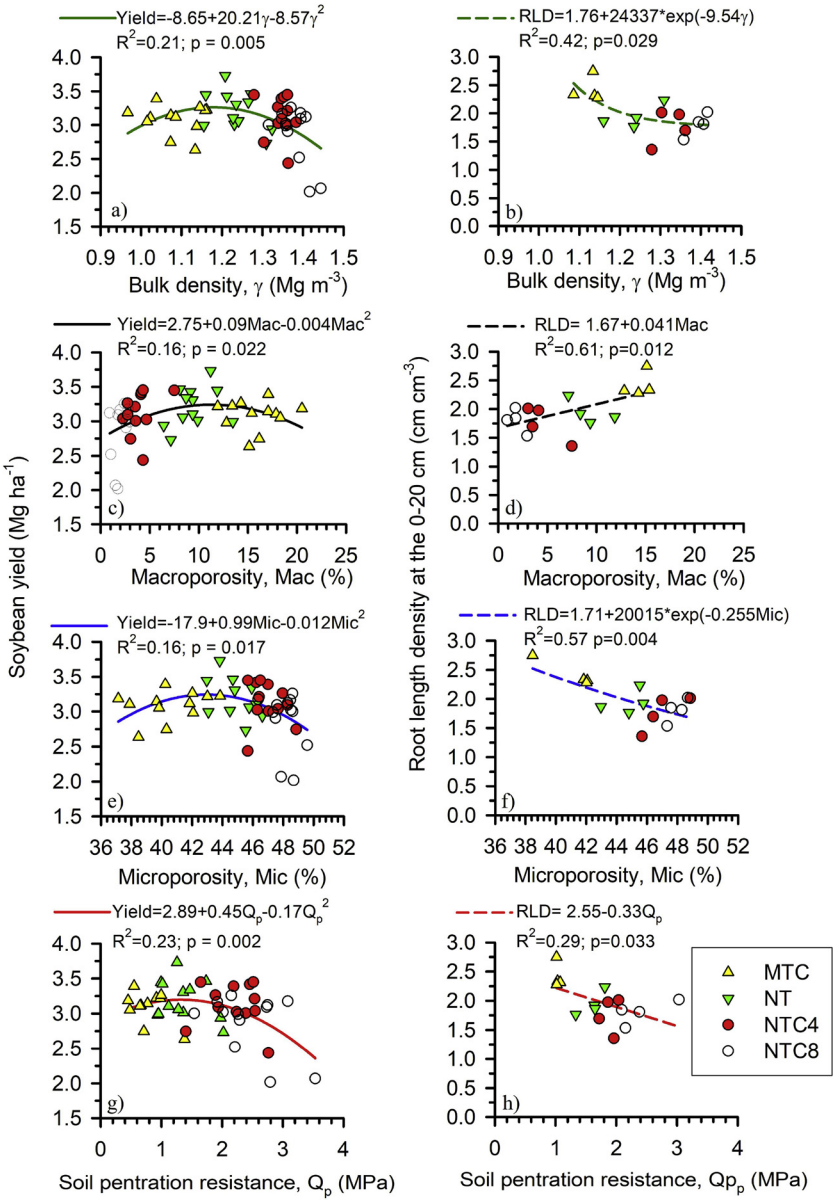

Fig. 7. Relation of soybean grain yield (yield) (a,c,e) and root length density (RLD) (b,d,e) with bulk density (γ) (a,b), macroporosity (Mac) (c,d), microporosity (Mic) (e,f) and soil penetration resistance (Q_p) (g,h) in 0 to 20 cm depth in a Rhodic Eutrudox. MTC: minimum tillage system with soil chiselling; NT: no-tillage system; and no-tillage with additional compaction by four passes of tractor (NTC4) or eight passes of harvester (NTC8).

depth. When the soil was compact, the time needed to reach 50 cm depth was increased to 50 days (NTC4 and NTC8). Thus, there was a reduction of soil volume that could be explored by roots so that less water was available for root uptake, and the time with stress conditions for plant development was increased. In addition, there were 25 days of drought during the reproductive phenological stage, which was from 30 November to 24 December of 2013. During those 25 days, there was only 29 mm of rainfall, totalizing 1.2 mm day^{-1}. However, in that time the potential evaporation was around 5.3 mm day^{-1} (134 mm). This indicated a severe water deficit restricting soybean grain yield.

3.6. Stress reduction function for root elongation

The influence of soil physical conditions to root growth was modelled by a stress reduction function (Fig. 10). The stress reduction function changes with soil penetration resistance and matric potential (poor aeration and water stress), and proportionally reduces the maximum root elongation. It is a function from one (maximum root growth) to zero (no growth), which changes with depth and time, thus, there is a different stress reduction affecting each individual root in the soil profile.

Rooting depth was restricted in compacted soils with slower root elongation due mechanical and hydric stresses. In compacted soils (by tractor or harvester) plants needed 13 days longer to reach 50 cm depth (Fig. 10c and d) compared to MTC (Fig. 10a). Mechanical and hydric stresses were related to soil and rainfall conditions during crop season. The rainfall was the same for all treatments. However, soil conditions were changed due to management effects, thus, there was a rainfall deficit in the reproductive stage. For example, from R1 to R5 there was 29 mm during 25 days (1.2 mm day^{-1}).

The total stress reduction function for root elongation (Fig. 11a) is divided into two mechanisms, penetration resistance stress (Fig. 11b) and matric potential stress (Fig. 11c). This shows a reduction of root length density due to soil physical limitations during the growth season. Fig. 11 indicates that, for all soil compaction levels, root elongation rate was smaller than 60 % of maximum elongation rate, and this was

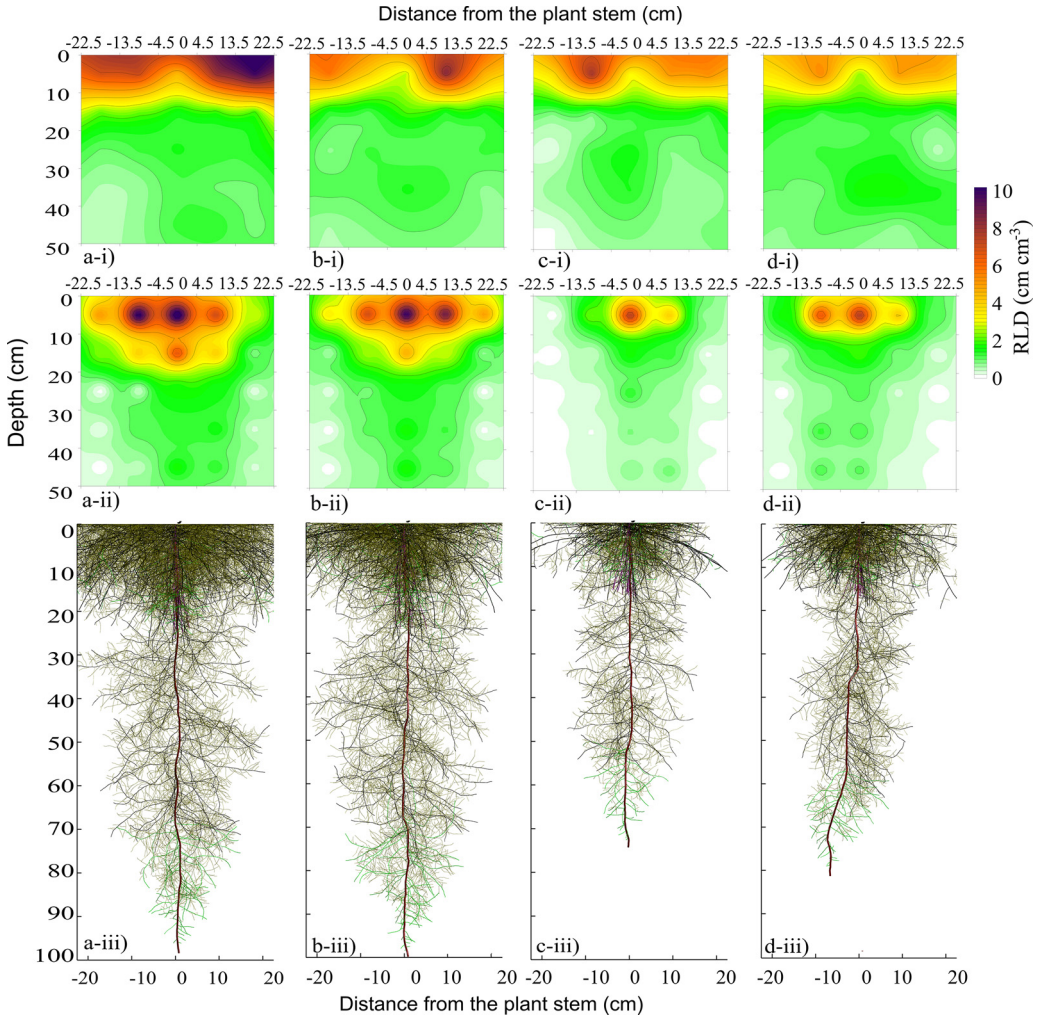

Fig. 8. 2D distribution of soybean root length density (RLD) measured at field (i) and simulated (ii) and its root system architecture simulated (iii) for minimum tillage system with soil chiselling (a), no-tillage system (b), and no-tillage with additional compaction by four passes of tractor (c) or eight passes of harvester (d) in an Oxisol. Dynamic root growing can be found at supplementary material, which are the videos of simulation scenarios for MTC (S1), NT (S2), NTC4 (S3) and NTC8 (S4).

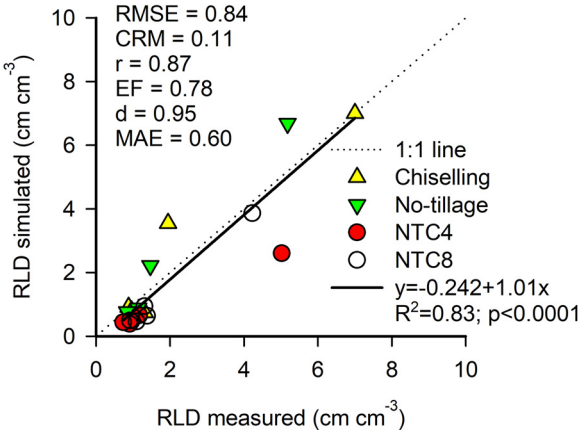

Fig. 9. Relation of root length density (RLD) simulated and measured of soybean in compaction levels of a Rhodic Eutrudox. MTC: minimum tillage system with soil chiselling; NT: no-tillage system; and no-tillage with additionally compaction by four passes of tractor (NTC4) or eight traffic of harvester (NTC8).

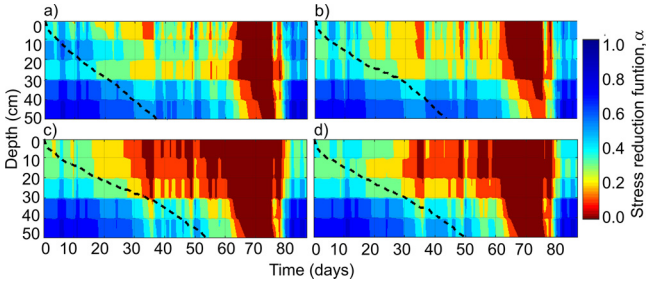

Fig. 10. Stress reduction function, α, for root elongation at the soil chiselling (a), no-tillage (b), NTC4 (c) and NTC8 (d) in a Rhodic Eutrudox during the root growing season. Dashed lines are the rooting depths over time for each soil compaction level. MTC: minimum tillage system with soil chiselling; NT: no-tillage system; and no-tillage with additionally compaction by four passes of tractor (NTC4) or eight traffic of harvester (NTC8).

mainly caused by stress due to penetration resistance.

3.7. Root anatomy

The general root shape of soybean under a no-tillage system was approximately circular in the primary (Fig. 12a–c) and in the secondary growing (Fig. 13a–c). However, under soil compaction it was flattened

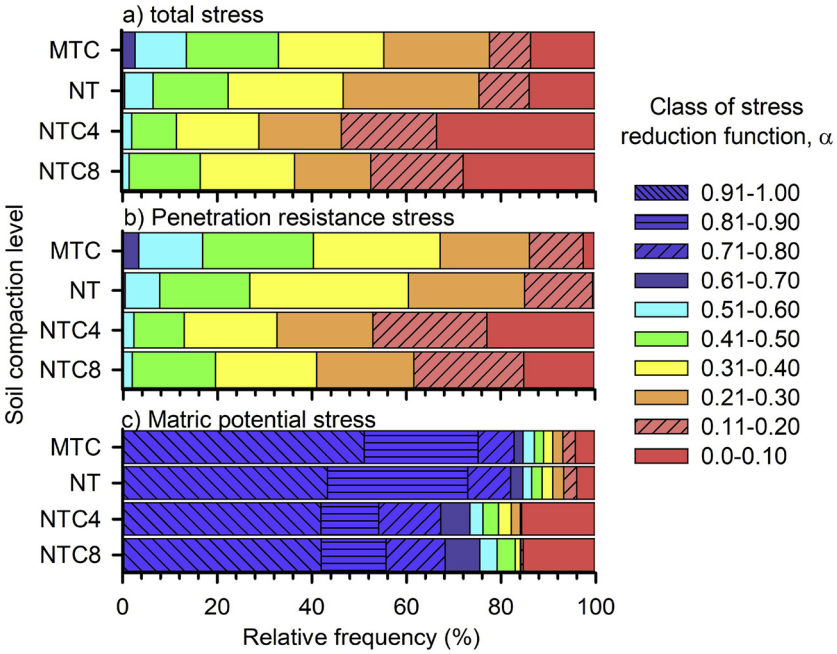

Fig. 11. Relative frequency of total stress reduction function, α, (a) and effect from soil penetration resistance (b) or matric potential (c) for soil chiselling, no-tillage (NT), NTC4 and NTC8 in soil profiles until 30 cm depth during the growing season of soybean. Stress reduction function near one is a maximum root elongation, and near zero, there is no root growth. MTC: minimum tillage system with soil chiselling; NT: no-tillage system; and no-tillage with additional compaction by four passes of tractor (NTC4) or eight passes of harvester (NTC8).

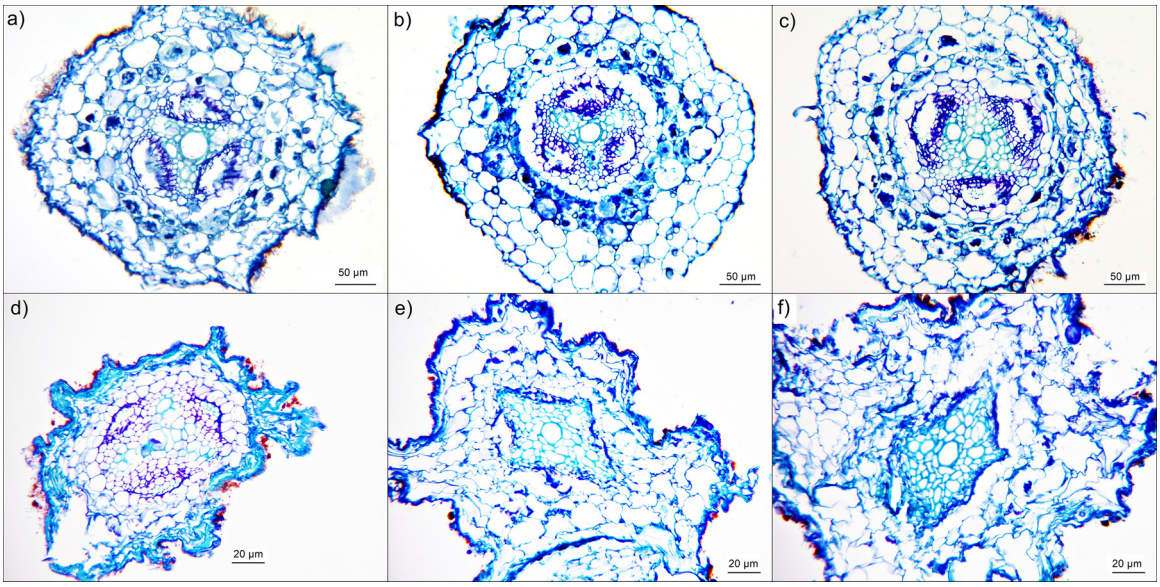

Fig. 12. Anatomy of soybean root at the primary tissues in no-tillage (a,b,c) and compacted soil by eight passes of harvester (d,e,f) in a Rhodic Eutrudox.

for all stages at the primary growth (Fig. 12d–f). The effect of stress on cell development is particularly complex, as abiotic stress is known to intervene in different aspects of cell development (Potters et al., 2009). Roots are efficient for adapting to stress conditions, especially with a prominent morphological and anatomical plasticity, resulting in cell deformation both in circular and flattened roots (Lipiec et al., 2012). Thus, different responses were observed for root anatomy, and the main effects were mechanical stress around the root cortex, and a few changes at the vascular cylinder. While our model does not describe root anatomy on this scale, root cross sections help us to actually see and understand how the stresses affect the root during its development.

4. Discussion

The modelling approach of Moraes et al. (2018) allows to simulate soybean root growth as a function of soil physical conditions, combining soil water flow modelling with macroscopic root water uptake from matric flux potential and dynamic effects of soil physical conditions on root elongation. The stress reduction function (Fig. 10) represented the soil condition for root growth of soybean under the conditions of four compaction levels in a Rhodic Eutrudox (Fig. 8) in a realistic way. The model improves our understanding of how the soil physical conditions contribute to the reduction of root growth (Fig. 10). Under loose soil conditions (i.e. MTC treatment), the tap root will reach a higher depth faster than in soils with compact layers as a result of less soil penetration resistance and soil physical limitation for root elongation. Consequently, the soil volume explored by such a root system is increased and this improves the soil water available for root uptake.

Soil-root interactions need detailed models to describe the impact of soil conditions on the biological development of plants (Vereecken et al., 2016). Other crop-soil models also describe the complex interaction, e.g. for water uptake (de Jong van Lier et al., 2008), stomatal resistance (Javaux et al., 2013), gravitropism, hydrotropism (Leitner et al., 2010) or chemotropism condition (Schnepf et al., 2012).

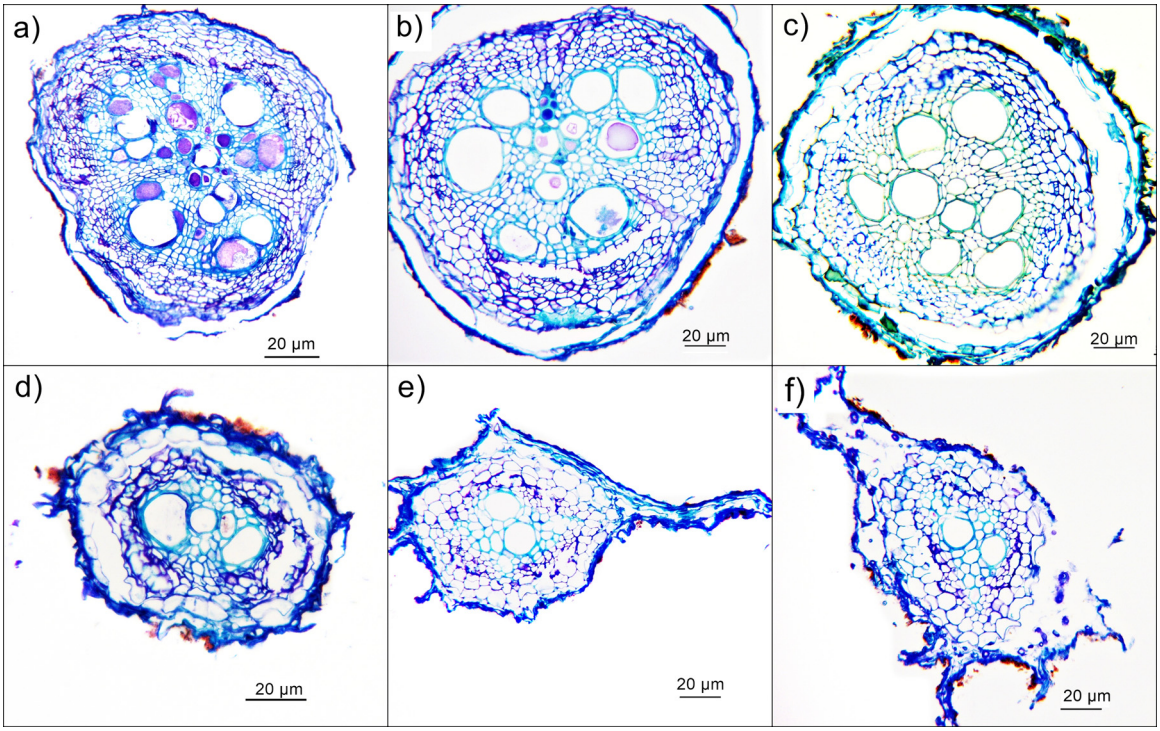

Fig. 13. Anatomy of soybean root at the secondary growing in no-tillage (a,b,c) and compacted soil by eight passes of harvester (d,e,f) in a Rhodic Eutrudox.

However, Moraes et al. (2018) were the first to describe the dynamics of soil physical processes for root growth, especially daily variation of soil penetration resistance, aeration and soil water content affecting root elongation. Their approach was shown to be applicable to the experimental conditions presented in this work.

Soybean yield and root growth in this very clayey Oxisol have low R-squared values in the equations related with static values for penetration resistance at field capacity (Fig. 7). However, all equations were very significant for p-values smaller than 5%. Even though these soil physical properties are easy to measure and interpret, being sensitive to differentiate the treatments that are related with yield and root development, they are static and do not reflect the underlying dynamics. Mathematical modelling is important to understand the mechanisms and soil physical conditions that affect crop development. Especially, impeded root elongation occurred due to the soil physical conditions changing with soil water dynamics during crop season (Fig. 10). In this respect, our model helps to understand the behaviour of soybean development as a function of soil structure and state. Soil chiselling affected the soil physical structure, increasing the total porosity and macroporosity (Fig. 2b, c), leading to decreased soil penetration resistance (Fig. 1), bulk density and microporosity (Fig. 2a, d). Root length density was increased with soil chiselling, especially down to 20 cm depth. However, soybean grain yield was reduced in relation to the no-tillage system. Thus, the soybean crop has more roots, equal shoot and less productivity than the no-tillage system, indicating that plant responses are a complex interaction within the soil-plant-atmosphere. In chiselled soil, soybean grain yield was reduced due to the changes in soil structure, such as the pore distribution (Fig. 2), water retention in micropores and especially due to the reduction of unsaturated hydraulic conductivity (Fig. 3), and increasing the total stress in top soil (Fig. 10a). Grain yield was affected stronger by soil chiselling in the top soil layer, due to less water supply from below because of a smaller soil unsaturated hydraulic conductivity (Calonego and Rosolem, 2010).

Soil compaction by agricultural traffic of tractor or harvester increased soil bulk density (Fig. 2) and penetration resistance (Fig. 1), while it decreased the soybean root length density in the compacted soil (Fig. 6b, c). Thus, the main effect of soil physical limitation for root growth and grain yield was observed in the compacted soil with eight passes of a harvest machine and with soil chiselling (Fig. 4). This indicates that soybean grain yield is reduced in loose soil and compacted soil (Fig. 7a), and the best condition for plant development and grain yield is the no-tillage system. Under no-tillage, continuous pores formed by decomposition of roots reduce the root resistance and are effective pathways that link the top soil with deeper layers (Calonego and Rosolem, 2010), improving the root proliferation depth yielding higher root water uptake than in soils without biopores (Jin et al., 2013).

Plant responses are a result of the interaction between environment and physical, chemical and biological soil conditions. This leads to low R-squared values in the equations which represent the relationship of soil physical attributes (bulk density, macroporosity, microporosity and soil penetration resistance) with grain yield or root length density (Fig. 7). This absence of a consistent relationship is due to soil physical conditions that change daily during the growth season, especially aeration, water content and soil penetration resistance which directly affect the plant development (Letey, 1985). Soil physical conditions are dynamic in time and space, especially soil penetration resistance increases exponentially with reduction of water content (Moraes et al., 2013). In general, crop responses are dependent on climatic conditions during the growing season, and the main possibility to explain the dynamic of soil physical conditions are by mathematical modelling of the underlying processes.

Soil-root interaction modelling improves the understanding of plant response to soil physical conditions (Fig. 11). Results regarding stress frequency during the growth season indicate that plants were exposed to different stresses due to soil penetration resistance and matric potential. The frequency of root growth reduction due to soil penetration resistance was higher when the soil compaction level was stronger. However, root growth in chiselled soils was strongly decreased by water stress (too little water for root growth), and due to unsaturated hydraulic conductivity (too slow water flow) (Fig. 3). The description of climate–soil–plant feedback helps to better understand the effect of cropping systems on soil quality (Bodner et al., 2015). Moreover soil-root modelling represents an important tool to explain the water use efficiency in various climatic conditions (Tron et al., 2015).

With moderate soil compaction, produced by tractor traffic, the soil physical conditions were changed, but this was not limiting for crop production, keeping the grain yield similar to the no-tillage system (Fig. 4). Nosalewicz and Lipiec (2014) studied how the soil compaction affects water uptake by roots, and their results indicated that heavily compacted soil layers increased stomatal resistance decreasing the total water uptake. However, the root water uptake rate decreased with higher root length density (Nosalewicz and Lipiec, 2014).

Soil physical limitation as a result of total stress (Fig. 11) reduced the crop yield (Fig. 4), and decreased the root elongation rate changing the root system by restricting rooting depth (Fig. 10), and changing the shape of the root growth anatomy in the primary structure (Fig. 12) as well as in the secondary root growth anatomy (Fig. 13). As a result of modelling soil physical conditions during the growing season (Fig. 10), root growth (Fig. 8 and supplementary videos, S1, S2, S3 and S4), plant transpiration (Fig. 5), and changes in the root anatomy (Figs. 12 and 13), can help to explain how roots develop considering weather variation and the resulting soil water flux into the soil. Root penetration into dense soil layers is possible with some physiological adaptations such as a stronger root cap protected by mucilage, which plays an important role protecting the root meristem from damage (Bengough, 2006). However, soil structure and pore continuity are the most important factors to keep up a high root elongation rate (Jin et al., 2013). Thus, different pedoclimatic conditions constrain root elongation because of soil strength and oxygen deficiency (Valentine et al., 2012). Additionally, cracks can reduce root-penetration resistance to only one-quarter of that which would be expected from the penetrometer measurement in the bulk soil (Bengough and Mullins, 1991). Bengough (2012) showed that root elongation rates are reduced only if the mechanical impedance is applied at the root tip with an axial pressure. For this reason, pore continuity as encountered in no-tillage systems is very important to accelerate and increase the root growth in deep soil profiles.

In the no-tillage system, secondary root growth had only few compressions around the root cells, however, for cells that expanded into a soil compartment with higher soil strength, the shape changed and the cortex cells were compressed mechanically to preserve the anatomic distribution of xylem and phloem at the vascular cylinder. In general, cells located in the vascular cylinder were found to expand, whereas those located around the cortex were found to be radially compressed. The function of xylem is transport (unidirectional) of water and nutrients from roots to the shoots (Costa et al., 2013). The phloem is responsible for translocation (bidirectional) of organic and mineral material from leaves to storage organs and growing parts of the plant (Machado and Carmello-Guerreiro, 2013). The secondary root growth starts when vascular cambium produces xylem and secondary phloem. Thus, the vascular cambium is formed from vascular tissues and phellogen originated from periderm (Queiroz-Voltan et al., 2000). Soil compaction changes the anatomy, shape and size of roots, and this can be seen in the deformation of cortex cells in the secondary root growth stage (Fig. 13). The vascular cylinder under the no-tillage condition has more xylems which have a larger cross section than under compacted soil conditions. The roots grown in compacted soil promoted rupturing of epidermal cells, and the cortical parenchyma cells were more spherical in agreement with Baligar et al. (1975). Thus, the soil compaction promoted changes in shape of vascular cylinder, which became oval shape in outline.

In general, the soil physical properties which directly affect root growth are dynamic over the growing season (e.g. soil water content, mechanical impedance and soil aeration). Thus, this model simulates root growth by coupling soil, root and weather to explain soil physical effects on plant development. Mechanical impedance in compacted soil can restrict rooting depth. In no-tillage and soil chiselled, the root growth was impeded by stress due to soil penetration resistance for less than 20 % of the time, while in compacted soils (NTC4 and NTC8) for more than 40 % of time. In the chiselling and no-tillage systems this promoted a faster root elongation rate than compacted soils resulting in a deeper root system than in areas with traffic of tractor or harvester.

5. Conclusion

In this study, we have shown the analysis of complex soil-root interactions investigating soil physical limitations to root growth by coupling root elongation, root water uptake and soil water flow. The application of the soil-root interaction model was performed successfully describing soybean crop development for different soil compaction scenarios of a Rhodic Eutrudox.

We measured soybean grain yield cropped in various compaction levels in an Oxisol, and applied mathematical modelling to get a very clear understanding how soil compaction affected root system development. Therefore, our model improved the fundamental understanding how the soil structure affects root growth under field conditions. Since the model can be applied for various pedoclimatic conditions, it will develop into a tool supporting agricultural management decisions and will play an increasingly important role in root-soil interaction research.

Mechanical stress has a major impact on soil-root interaction for root growth under compacted soil conditions. Hydric stress increases the soil physical limitation to root growth under soil chiselling conditions. Soil chiselling increases root length density, but reduces grain yields. Thus, soybean grain yield was reduced due to both soil chiselling and heavy traffic.

Declaration of Competing Interest

The authors declare that this research was conducted in the absence of any commercial or financial relationships that could be construed as a potential conflict of interest.

Acknowledgements

MTM appreciates the scholarship funded by the Brazilian Federal Agency for Support and Evaluation of Graduate Education (CAPES) to stay at the James Hutton Institute, in Dundee, UK, for 12 months as a visiting PhD student (Process n° BEX 2934/15-9). This study has also received funding from the Agrisus Foundation (PA n° 1236/13). This research was partially funded by the Deutsche Forschungsgemeinschaft (DFG, German Research Foundation) under Germany's Excellence Strategy - EXC 2070 – 390732324.

Appendix A. Supplementary data

Supplementary material, about dynamic of root growing and stress reduction funtion over season growth can see observed for minimum tillage system with soil chiselling (supplementary video, S1), no-tillage system (supplementary video, S2), and no-tillage with additional compaction by four passes of tractor (supplementary video, S3) or eight passes of harvester (supplementary video, S4), related to this article can be found, in the online version, at doi:https://doi.org/10.1016/j.still.2020.104611.

References

Addiscott, T.M., Whitmore, A.P., 1987. Computer simulation of changes in soil mineral nitrogen and crop nitrogen during autumn, winter and spring. J. Agric. Sci. 109, 141–157.
Allen, R.G., Pereira, L.S., Raes, D., Smith, M., 1998. Crop Evapotranspiration: Guidelines for Computing Crop Requirements. Irrig. Drain. Pap. No. 56. FAO 300.
Alvares, C.A., Stape, J.L., Sentelhas, P.C., de Moraes Gonçalves, J.L., Sparovek, G., 2013. Köppen's climate classification map for Brazil. Meteorol. Z. 22, 711–728.
Baligar, V.C., Nash, V.E., Hare, M.L., Price, J.A., 1975. Soybean root anatomy as influenced by soil bulk density1. Agron. J. 67, 842.
Bengough, A.G., 1997. Modelling rooting depth and soil strength in a drying soil profile. J. Theor. Biol. 186, 327–338.

Bengough, A.G., 2006. Root responses to soil physical conditions; growth dynamics from field to cell. J. Exp. Bot. 57, 437–447.
Bengough, A.G., 2012. Root elongation is restricted by axial but not by radial pressures: So what happens in field soil? Plant Soil 360, 15–18.
Bengough, A.G., Mullins, C.E., 1991. Penetrometer resistance, root penetration resistance and root elongation rate in two sandy loam soils. Plant Soil 131, 59–66.
Bengough, A.G., McKenzie, B.M., Hallett, P.D., Valentine, T.A., 2011. Root elongation, water stress, and mechanical impedance: a review of limiting stresses and beneficial root tip traits. J. Exp. Bot. 62, 59–68.
Bodner, G., Nakhforoosh, A., Kaul, H.P., 2015. Management of crop water under drought: a review. Agron. Sustain. Dev. 35, 401–442.
Böhm, W., 1979. Methods of Studying Root Systems, Biological Conservation, Ecological Studies. Springer Berlin Heidelberg, Berlin.
Bonfante, A., Basile, A., Acutis, M., De Mascellis, R., Manna, P., Perego, A., Terribile, F., 2010. SWAP, CropSyst and MACRO comparison in two contrasting soils cropped with maize in Northern Italy. Agric. Water Manage. 97, 1051–1062.
Busscher, W.J., 1990. Adjustment of flat-tipped penetrometer resistance data to a common water content. Trans. ASAE 33, 0519–0524.
Calonego, J.C., Rosolem, C.A., 2010. Soybean root growth and yield in rotation with cover crops under chiseling and no-till. Eur. J. Agron. 33, 242–249.
Casaroli, D., de Jong van Lier, Q., Dourado Neto, D., 2010. Validation of a root water uptake model to estimate transpiration constraints. Agric. Water Manage. 97, 1382–1388.
Chen, G., Weil, R.R., 2011. Root growth and yield of maize as affected by soil compaction and cover crops. Soil Tillage Res. 117, 17–27.
Costa, C., Dwyer, L.M., Hamilton, R.I., Hamel, C., Nantais, L., Smith, D.L., 2000. A sampling method formeasurement of large root systems with scanner-based Image analysis. Agron. J. 92, 621–627.
Costa, C.G., Callado, C.H., Coradin, V.T.R., Carmello-Guerreiro, S.M., 2013. Xilema. In: Appezzatto-da-Glória, B., Carmello-Guerreiro, S.M. (Eds.), Anatomia Vegetal. Editora UFV, Viçosa, pp. 123–133.
de Jong van Lier, Q., van Dam, J.C., Metselaar, K., de Jong, R., Duijnisveld, W.H.M., 2008. Macroscopic root water uptake distribution using a matric flux potential approach. Vadose Zone J. 7, 1065–1078.
Dresbøll, D.B., Thorup-Kristensen, K., McKenzie, B.M., Dupuy, L.X., Bengough, A.G., 2013. Timelapse scanning reveals spatial variation in tomato (*Solanum lycopersicum* L.) root elongation rates during partial waterlogging. Plant Soil 369, 467–477.
Embrapa, 2011. Tecnologias de produção de soja - Região Central do Brasil 2012 e 2013, 15th ed. Embrapa Soja, Londrina 212p.
Iijima, M., Kato, J., 2007. Combined soil physical stress of soil drying, Anaerobiosis and mechanical impedance to seedling root growth of four crop species. Plant Prod. Sci. 10, 451–459.
Javaux, M., Couvreur, V., Vanderborght, J., Vereecken, H., 2013. Root water uptake: from three-dimensional biophysical processes to macroscopic modeling approaches. Vadose Zone J. 12 vzj2013.02.0042.
Jin, K., Shen, J., Ashton, R.W., Dodd, I.C., Parry, M.A.J., Whalley, W.R., 2013. How do roots elongate in a structured soil? J. Exp. Bot. 64, 4761–4777.
Jorge, L.A.C., Silva, D.J.C.B., 2010. Safira: manual de utilização. Embrapa Istrumentação Agropecuária, São Carlos, SP, 1a ed. .
Keller, T., da Silva, A.P., Tormena, C.A., Giarola, N.F.B., Cavalieri, K.M.V., Stettler, M., Arvidsson, J., 2015. SoilFlex-LLWR: linking a soil compaction model with the least limiting water range concept. Soil Use Manage. 31, 321–329.
Leitner, D., Klepsch, S., Bodner, G., Schnepf, A., 2010. A dynamic root system growth model based on L-systems. Plant Soil 332, 177–192.
Letey, J., 1985. Relationship between soil physical properties and crop production. Adv. Soil Sci. 1, 277–294.
Lipiec, J., Horn, R., Pietrusiewicz, J., Siczek, A., 2012. Effects of soil compaction on root elongation and anatomy of different cereal plant species. Soil Tillage Res. 121, 74–81.
Machado, S.R., Carmello-Guerreiro, S.M., 2013. Floema. In: Appezzato-da-Glória, B., Carmello-Guerreiro, S.M. (Eds.), Anatomia Vegetal. Editora UFV, Viçosa, pp. 147–153.
Moraes, M.T., 2017. Root Growth Modelling of Corn and Soybean Affected by Hydric and Mechanical Stress in Oxisol (Ph.D). 122p. Available at. Federal University of Rio Grande do Sul. http://hdl.handle.net/10183/156643.
Moraes, M.T., Debiasi, H., Franchini, J.C., Silva, V.R., 2013. Soil penetration resistance in a rhodic eutrudox affected by machinery traffic and soil water content. Eng. Agrícola 33, 748–757.
Moraes, M.T., Debiasi, H., Carlesso, R., Franchini, J.C., Silva, V.R., 2014a. Critical limits of soil penetration resistance in a rhodic Eutrudox. Rev. Bras. Ciênc. Solo 38, 288–298.
Moraes, M.T., Silva, V.R., Zwirtes, A.L., Carlesso, R., 2014b. Use of penetrometers in agriculture: a review. Eng. Agrícola 34, 179–193.
Moraes, M.T., Debiasi, H., Carlesso, R., Franchini, J.C., Silva, V.R., Luz, F.B., 2016. Soil physical quality on tillage and cropping systems after two decades in the subtropical region of Brazil. Soil Tillage Res. 155, 351–362.
Moraes, M.T., Debiasi, H., Carlesso, R., Franchini, J.C., Silva, V.R., Luz, F.B., 2017. Age-hardening phenomena in an oxisol from the subtropical region of Brazil. Soil Tillage Res. 170, 27–37.
Moraes, M.T., Bengough, A.G., Debiasi, H., Franchini, J.C., Levien, R., Schnepf, A., Leitner, D., 2018. Mechanistic framework to link root growth models with weather and soil physical properties, including example applications to soybean growth in Brazil. Plant Soil 428 (1-2), 67–92.
Moraes, M.T., Debiasi, H., Franchini, J.C., Bonetti, J., de, A., Levien, R., Schnepf, A., Leitner, D., 2019. Mechanical and hydric stress effects on maize root system development at different soil compaction levels. Front. Plant Sci. 10, 1358. https://doi.org/10.3389/fpls.2019.01358.
Mualem, Y., 1976. A new model for predicting the hydraulic conductivity of unsaturated porous media. Water Resour. Res. 12, 513–522.
Nosalewicz, A., Lipiec, J., 2014. The effect of compacted soil layers on vertical root distribution and water uptake by wheat. Plant Soil 375, 229–240.
Nunes, M.R., Denardin, J.E., Pauletto, E.A., Faganello, A., Pinto, L.F.S., 2015. Mitigation of clayey soil compaction managed under no-tillage. Soil Tillage Res. 148, 119–126.
O'Sullivan, M.F., Henshall, J.K., Dickson, J.W., 1999. A simplified method for estimating soil compaction. Soil Tillage Res. 49, 325–335.
O'Brien, T.P., Feder, N., McCully, M.E., 1964. Polychromatic staining of plant cell walls by toluidine blue O. Protoplasma 59, 368–373. https://doi.org/10.1007/BF01248568.
Ortigara, C., 2017. Physical and Hydric Properties of a Rhodic Eutrudox in Different Long-Term Crop Systems (Master's Dissertation). 75p. Available at. Federal University of Santa Maria. http://repositorio.ufsm.br/handle/1/11554.
Potters, G., Pasternak, T.P., Guisez, Y., Jansen, M.A.K., 2009. Different stresses, similar morphogenic responses: integrating a plethora of pathways. Plant Cell Environ. 32, 158–169.
Queiroz-Voltan, R.B., Nogueira, S.D.S.S., Miranda, M.A.C., 2000. Aspectos da estrutura da raiz e do desenvolvimento de plantas de soja em solos compactados. Pesqui. Agropecu. Bras. 35, 929–938.
Rabot, E., Wiesmeier, M., Schlüter, S., Vogel, H.J., 2018. Soil structure as an indicator of soil functions: a review. Geoderma 314, 122–137.
Reichert, J.M., Suzuki, L.E.A.S., Reinert, D.J., Horn, R., Hakansson, I., 2009. Reference bulk density and critical degree-of-compactness for no-till crop production in subtropical highly weathered soils. Soil Tillage Res. 102, 242–254.
Saglio, P.H., Rancillac, M., Bruzan, F., Pradet, A., 1984. Critical oxygen pressure for growth and respiration of excised and intact roots. Plant Physiol. 76, 151–154.
SAS, I.I, 2013. SAS Enterprise Guide.
Schnepf, A., Leitner, D., Klepsch, S., 2012. Modeling phosphorus uptake by a growing and exuding root system. Vadose Zone J. 11, 318–327.
Tron, S., Bodner, G., Laio, F., Ridolfi, L., Leitner, D., 2015. Can diversity in root architecture explain plant water use efficiency? A modeling study. Ecol. Modell. 312, 200–210.
Valentine, T.A., Hallett, P.D., Binnie, K., Young, M.W., Squire, G.R., Hawes, C., Bengough, A.G., 2012. Soil strength and macropore volume limit root elongation rates in many UK agricultural soils. Ann. Bot. 110, 259–270.
van Dam, J.C., Feddes, R.A., 2000. Numerical simulation of infiltration, evaporation and shallow groundwater levels with the Richards equation. J. Hydrol. 233, 72–85.
van Genuchten, M.T., 1980. A closed-form equation for predicting the hydraulic conductivity of unsaturated soils. Soil Sci. Soc. Am. J. 44, 891–898.
Vereecken, H., Schnepf, A., Hopmans, J.W., Javaux, M., Or, D., Roose, T., Vanderborght, J., Young, M.H., Amelung, W., Aitkenhead, M., Allison, S.D., Assouline, S., Baveye, P., Berli, M., Brüggemann, N., Finke, P., Flury, M., Gaiser, T., Govers, G., Ghezzehei, T., Hallett, P., Hendricks Franssen, H.J., Heppell, J., Horn, R., Huisman, J.A., Jacques, D., Jonard, F., Kollet, S., Lafolie, F., Lamorski, K., Leitner, D., McBratney, A., Minasny, B., Montzka, C., Nowak, W., Pachepsky, Y., Padarian, J., Romano, N., Roth, K., Rothfuss, Y., Rowe, E.C., Schwen, A., Šimůnek, J., Tiktak, A., Van Dam, J., van der Zee, S.E.A.T.M., Vogel, H.J., Vrugt, J.A., Wöhling, T., Young, I.M., 2016. Modeling soil processes: review, key challenges, and new perspectives. Vadose Zone J. 15 vzj2015.09.0131.
Willmott, C.J., Robeson, S.M., Matsuura, K., 2012. A refined index of model performance. Int. J. Climatol. 32, 2088–2094.